energies

MDPI

Article

Development of a Variable Valve Actuation Control to Improve Diesel Oxidation Catalyst Efficiency and Emissions in a Light Duty Diesel Engine

José R. Serrano, Francisco J. Arnau *, Jaime Martín and Ángel Auñón

CMT—Motores Térmicos, Universitat Politècnica de València, Camino de Vera s/n, 46022 Valencia, Spain; jrserran@mot.upv.es (J.R.S.); jaimardi@mot.upv.es (J.M.); ngeaugar@mot.upv.es (Á.A.)

* Correspondence: farnau@mot.upv.es

Received: 29 July 2020; Accepted: 25 August 2020; Published: 3 September 2020

Abstract: Growing interest has arisen to adopt Variable Valve Timing (VVT) technology for automotive engines due to the need to fulfill the pollutant emission regulations. Several VVT strategies, such as the exhaust re-opening and the late exhaust closing, can be used to achieve an increment in the after-treatment upstream temperature by increasing the residual gas amount. In this study, a one-dimensional gas dynamics engine model has been used to simulate several VVT strategies and develop a control system to actuate over the valves timing in order to increase diesel oxidation catalyst efficiency and reduce the exhaust pollutant emissions. A transient operating conditions comparison, taking the Worldwide Harmonized Light-Duty Vehicles Test Cycle (WLTC) as a reference, has been done by analyzing fuel economy, HC and CO pollutant emissions levels. The results conclude that the combination of an early exhaust and a late intake valve events leads to a 20% reduction in CO emissions with a fuel penalty of 6% over the low speed stage of the WLTC, during the warm-up of the oxidation catalyst. The same set-up is able to reduce HC emissions down to 16% and NO_x emission by 13%.

Keywords: variable valve actuation; variable valve timing; light-duty diesel engine; aftertreatment thermal management; one- dimensional model; world harmonized light-duty vehicle test procedure; light-off temperature; diesel engine emissions

1. Introduction

During the last years, the emissions legislation in the major automotive regions have established more restrictive limits of the air pollutants released into the atmosphere in order to reduce the environmental impact of the transportation activities. To this end, minimizing fuel consumption and emissions has become one of the major goals of engine developers and manufacturers. Especially in diesel engines, a great challenge is the cold start and heating phase, since heating techniques are a compromise between a fast heat-up of the after-treatment system and a low penalty in fuel consumption.

Several studies have been performed addressing the topic of the exhaust thermal management. Arnau et al. [1] studied the potential that variable valve timing and a second exhaust valve event have in increasing the exhaust gas temperature. Their results showed that an increment of 50 °C in the exhaust temperature, associated with a fuel penalty of 5%, can be obtained by advancing the exhaust and delaying the intake valve events. Luján et al. [2] studied the possibility of placing the after-treatment system, a DOC (Diesel Oxidation Catalyst) coupled to a DPF (Diesel Particle Filter), before the turbine to ease the pollutants oxidation and DPF passive regeneration.

Concerning the fuel consumption improvements, VVT has commonly been widely used in spark ignited (SI) engines rather than in compression ignited (CI) engines. At low loads, the pumping

losses in gasoline engines are greater than those of diesel engines because of the intake throttling. Without a throttle valve, the control of the air-fuel mixture can be achieved by variation of the intake valve opening period; therefore, the VVT has great potential for reducing pumping losses in gasoline engines. In diesel engines, whose control of load is performed by regulating the amount of fuel injected, pumping losses at partial loads are lower. The application of VVT in diesel engines is restricted due to the small clearance height between piston and cylinder head at top dead center (TDC), which allows reaching higher compression ratios than in gasoline engines. This restriction means that the valves can have a little or no lift at overlap TDC, which involves a reduced margin for advancing the intake opening and retarding the exhaust closing in order to avoid valve to piston contact. Contrarily, there are no restrictions regarding the exhaust opening and intake closing events. As a consequence, conventional camshaft phasers are used very little in diesel engines, but systems that provide control over the valve open period can be used [3].

However, in order to optimize the cold start and the heating phase, VVT applications have shown a great potential in diesel engines, making it possible to provide the residual gas required for this situation [4,5]. This leads to a reduction of carbon monoxide (CO) and hydrocarbons (HC) emissions that are intrinsic to the cold start.

In this paper, a simulation study is presented comparing different exhaust valve actuation strategies in order to increase the exhaust temperature of a light-duty diesel engine. A parametric study in steady-state conditions has been carried to develop a control strategy to define the optimal valve timing parameters (EVO advance, re-opening lift, etc.) for each operating point. Five control strategies have been tested in real driving conditions and they are discussed and compared in this work.

1.1. Valve Events of a Four-Stroke Engine

Figure 1 shows the valve timing diagram of a conventional light-duty diesel engine. In that diagram, one can differentiate four valve events: intake opening and closing (IVO and IVC) and exhaust opening and closing (EVO and EVC).

1.2. Variable Valve Timing Strategies

The four different valve events that are described above are fixed in conventional cam actuation system. Thus, the timing of these valve events is the result of a performance compromise under different operating conditions. Variable valve timing strategies arise from the need to find the most efficient way to operate the engine depending on its engine speed and load at any point of the engine map. Consequently, different approaches can be described by advancing or delaying the different valve events:

1.2.1. Intake Valve Opening (IVO)

By advancing the IVO event (early IVO or EIVO), intake valve opens before TDC during the exhaust stroke. Thus, increasing the valve overlap and the amount of burnt gases backflow into the intake ports. This part of exhaust gases mixes with fresh air from the intake manifold and serves as an internal gas recirculation (IGR), reducing the combustion temperature and, consequently, reducing the NO_x amount [6] produced during the combustion. Experiments that were carried out by Tomoda et al. [7], in a 2.2 litres Diesel engine, found that advancing the IVO timing before TDC results in an improvement of the swirl ratio and an increase in the introduced air mass at low and high load. This effect leads to a better trade-off between NO_x and fuel consumption. The fuel economy improvement is produced and enhanced combustion rate due to the higher swirl ratio and the reduction in pumping losses due to early IVO [7].

The duration of the valve overlap depends on several factors: the distance between piston and cylinder head at TDC (which usually is lower in a diesel engine due to the high compression ratio), the engine speed and the instantaneous pressures at intake and exhaust ports. In diesel engines, when pressure is higher in exhaust manifold, valve overlap should be reduced in order to avoid

backflows into intake manifold [8]. Delaying the IVO (LIVO) event reduces valve overlap, leading to a very low or insignificant backflow into intake manifold. Deppenkemper et al. [9] found, using a one-dimensional engine model, that if the IVO is delayed up to the beginning of the intake stroke, the velocity at which the air enters into the cylinder will be higher due to the lower pressure inside the cylinder. This increase in inlet air velocity enhances in-cylinder turbulence, which improves the mixing process, which results in lower HC emissions.

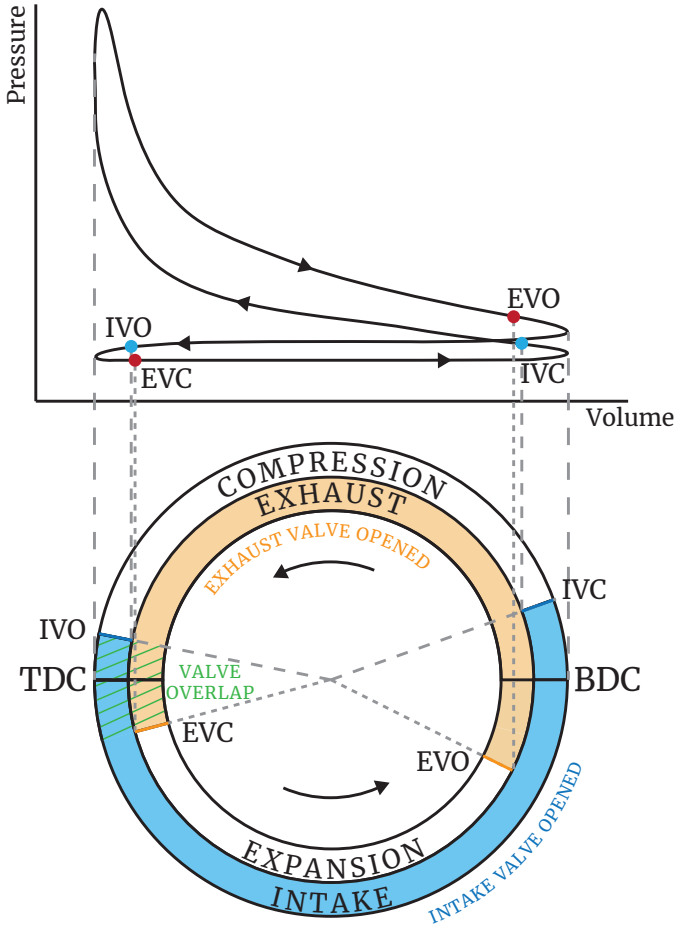

Figure 1. Four stroke diesel engine P-V diagram (top) and engine timing diagram (bottom).

1.2.2. Intake Valve Closing (IVC)

Backflow during the compression stroke can be reduced or avoided by advancing IVC. Early IVC (EIVC) strategy reduces the amount of air admitted into the cylinder and thereby slightly reduces the work that is required for filling the cylinder when compared with a conventional valve timing. Zammit et al. [10] found that EIVC decreases NO_x emissions for advances greater than 30° CA at low engine speeds and low loads, reduces soot levels and raises exhaust gas temperatures. Nevertheless, CO and HC engine-out emissions increases and fuel economy is deteriorated, since more fuel amount is required for a lower air charge [10]. Tomoda et al. [7] also claim that when the IVC timing is advanced towards bottom dead center (BDC), the effective compression ratio increases, and this creates an increased compression end temperature, so that HC formation is reduced. The increase in effective compression ratio also allows for an increase of EGR (Exhaust Gases Recirculation) rate, resulting in reduced NO_x emissions. At high loads, however, EIVC decreases the amount of charged air mass in the cylinder and results in an increase of HC emissions. According to Tomoda et al. [7], early IVC on one intake valve relative to the other valve allows controlling the swirl strength, resulting in A NO_x and

soot emissions reduction at high load because it reduces both pumping losses and fuel consumption. In gasoline engines, Pan et al. [11] studied the improvement on the brake thermal efficiency by the application of the Miller cycle. Their results prove that after Miller cycle application, the pumping loss is improved, and the combustion duration can be reduced by advancing the ignition timing.

On the contrary, performing a late intake valve closing means that intake valves are opened during the first part of the compression stroke. Consequently, some of the air flows back into the intake manifold, leading to a reduction in the effective compression ratio and a lambda reduction (lower combustion chamber charge). These two consequences lead to a higher exhaust gas temperatures and a NO_x engine-out emission reduction [12–14]. However, Maniatis et al. [15] experiments did not find any advantage in exhaust gas enthalpy or a reduction of HC and CO emissions. Kim et al. [16] found that the amount of EGR could be reduced to maintain a similar level of NO_x emissions when the IVC timing is retarded. This characteristic also prevents an increase in soot emissions. The combination of EGR and LIVC helped to improve the NO_x-soot trade-off relation [13,14]. Similarly, Zhou et al. [17] achieved a reduction in particle matter emissions by 32.9%, with a small increase in NO_x by applying LIVC strategy and an optimal control of the VGT (Variable Geometry Turbine) and EGR during realistic transient conditions.

1.2.3. Exhaust Valve Opening (EVO)

The early opening of the exhaust valve provides better scavenging of the exhaust gases, but it also causes a reduction in the expansion work, resulting in a reduction of the engine brake power, thus worsening the fuel consumption. EEVO also produces an increment in exhaust pressure and temperature levels higher than those that were obtained with the standard valve timing. The greater the advance in EVO, the larger increment in exhaust temperature, but with a larger penalty in terms of BSFC [12,18]. Regarding pollutant emissions, EEVO results in an increase in engine-out hydrocarbons and CO, because their oxidation during the expansion stroke is interrupted with the early EVO [6,19]. In studies that were carried out by Gossala et al. [18] at idle conditions, the fuel penalty caused by early EVO produces more NO_x and particle matter emissions due to the higher injected fuel mass. Particle matter emissions can be reduced by increasing the air-fuel ratio, but it also reduces the exhaust temperature increment.

When delaying the exhaust valve opening (LEVO), the exhaust valve is opened near BDC or after this point. In this case, a greater expansion work is produced without losses during the power stroke. However, exhaust pumping work increases, because of a very late EVO, which results in some restriction to expel the exhaust gases out of the cylinder. According to Piano [12], a fast opening lift of the exhaust valve is usually desirable in order to retard the EVO timing while not penalizing BSFC. Moreover, an exhaust valve faster opening may also reduce the blow-down flow losses increasing the energy available at turbine inlet, especially needed at low engine speed where the variable geometry turbine is usually closed.

1.2.4. Exhaust Valve Closing (EVC)

In conventional diesel engines, EVC takes place at around 20° CA after TDC. Advancing this event prevents partially or totally valve overlap, which reduces or avoids the backflow of burnt gases through intake valves. This way, early EVC (EEVC) aids in retaining a portion of burnt gases inside the cylinder, which results in a reduction of engine-out NO_x and HC emissions [6]. Nonetheless, this strategy has some limitation to be applied on passenger vehicles as some authors reported an audible noise when the compressed exhaust gases eject into the intake manifold [15].

The exhaust valves are closed well after TDC, increasing the valve overlap period, in order to perform a late EVC (LEVC). This long overlap during the intake stroke results in some part of the burnt gases flowing back into the cylinder, creating an internal gas recirculation. Regarding engine-out pollutant emissions, NO_x and HC emissions are reduced when performing LEVC due to the IGR [6].

Because of the small clearance height between piston and cylinder head at TDC in CI engines, LEVC and EIVO are quite limited. This is also the reason why the application of VVT is more restricted in CI engines than in SI engines.

At high engine speed, the time in which both valves are opened is less than at low engine speed. In order to provide higher engine power output, a high valve overlap is beneficial for scavenging of residual gases, since the higher inertia of the gases at high engine speed allows for removing residual gases from the cylinder and increases volumetric efficiency. However, a large valve overlap is detrimental for low engine speed torque due to the larger amount of residual gases flowing back into the intake manifold.

Variable valve timing (VVT) strategies usually consist of a combination of the different sub-strategies mentioned above, like, for instance, phasing the exhaust; which can be a combination of EEVO and EEVC or, on the other side, a combination of LEVO and LEVC. Moreover, there are other different strategies in order to add flexibility to the engine valve train. By modifying valve lift, it is also possible to perform different opening-and-closing valve events along the engine cycle. These systems are called variable valve actuation (VVA).

It is known that IGR can increase the exhaust gas temperature and reduce engine-out emissions. This is done with the aid of a charge composition control achieved by an exhaust valve post-lift (or exhaust valve re-opening, EVrO) or an intake valve pre-lift during the exhaust stroke [8,20].

Intake valve pre-lift consists of a previous intake valve opening event during the exhaust stroke. The aim is to create a backflow of exhaust gases into the intake manifold that are re-entrained later during the intake stroke. On the contrary, the exhaust valve re-opening consists of a secondary exhaust valve opening event during the intake stroke. The vacuum that is created by the downward movement of the piston creates a backflow of exhaust gases from the exhaust manifold into the cylinder. Benajes et al. [8] found that the IGR amount achieved is higher when performing an exhaust valve post-lift than in the case of an intake valve pre-lift, with the advantage of recirculating the same amount exhaust gases independently of the speed and load.

2. Experimental Setup

This work has been performed based on a calibrated and validated HSDI Diesel engine model. This engine is a 1.6 L four-stroke engine compliant with Euro 5 emissions regulations whose specifications can be found in Table 1. From the point of view of thermal management, the low pressure EGR is cooled by a gas-coolant heat exchanger, and another gas-coolant heat exchanger cools the intake air to the cylinders. In order to reduce the warm-up time, the thermostat electrovalve blocks the coolant flow through the engine block during engine warming. The turbocharger system consists of a radial compressor and a variable geometry turbine (VGT). This turbocharger is not cooled by water, but all of the heat coming from the turbine and mechanical losses are dissipated by the lubricating oil. Finally, the after-treatment system consists of a close-coupled DOC and DPF brick.

Table 1. Engine specifications.

Type	EURO 5 HSDI Diesel Engine
Displacement	1598 cm^3
Stroke	79.5 mm
Bore	80 mm
Compression ratio	14.5:1
Number of valves	4 per cylinder (2 int., 2 exh.)
Number of cylinders	4 in line
Air management	VGT, LP-EGR, HP-EGR
EAT System	Closed-coupled DOC + DPF
Max. power @ speed	96 kW @ 4000 rpm
Max. torque @ speed	320 Nm @ 1750 rpm

The test cell consists of a climate dynamic room, which allows performing cold start tests (up to −15 °C). The test cell is fully equipped in order to measure operation mean variables and in-cylinder pressures in the four cylinders. It also includes a Horiba MEXA-One exhaust gas analyzer along with an AVL439 Opacimeter. Table 2 summarizes the relevant instruments used for this study. Data were acquired at a frequency of 10 Hz with a test automation system.

Table 2. Test cell instrumentation.

Variable	Instrument	Range	Accuracy
Crank angle	Encoder	0–360°	±0.02°
Torque	Dynamometer	0–400 Nm	±0.5 Nm
Gas/wall temperature	k-type thermocouple	70–1520 K	±2 K
Air mass flow	Sensyflow DN80	0–1700 hg/h	±2%
Coolant flow	Krohne 400 Optiflux	4.5–90 L/min	±0.5%
Oil pressure	Piezoresistive transducer	0–10 bar	±25 mbar
In-cylinder pressure	AVL GH13P	0–200 bar	Linearity 0.3%
Opacity	AVL439 Opacimeter	0–100%	0.01%
CO	Horiba MEXA-One	0–5000 ppm, 0–12 vol%	1% FS
CO_2	Horiba MEXA-One	0–20 vol%	1% FS
O_2	Horiba MEXA-One	0–22 vol%	1% FS
THC	Horiba MEXA-One	0–20,000 ppmC	1% FS
NO/NO_x	Horiba MEXA-One	0–10,000 ppm	1% FS

The engine layout is depicted in Figure 2, where the main components of the engine and the temperature and pressure measurement points are indicated. These points correspond to the intake and exhaust manifolds, and the inbound and outbound ducts of both compressor and turbine. The pollutant emissions points were measured upstream the after-treatment system, in order to calibrate the emissions sub-model. For the validation of the DOC and DPF sub-models, exhausts were measured upstream and downstream the after-treatment system, as explained by Payri et al. [21].

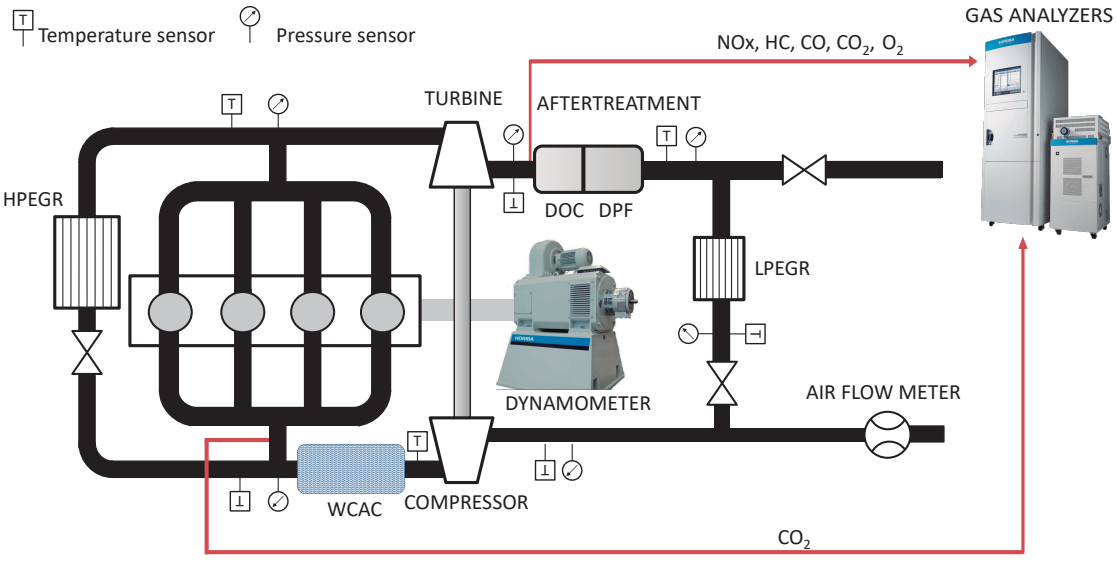

Figure 2. Engine layout indicating the pressure, temperature and exhaust gases measurement points.

3. Model Setup and Validation

This section addresses the engine model used throughout this work. First, the virtual engine model software is introduced, briefly presenting the different sub-models that make up the engine model. Finally, the validation process at transient operating conditions is discussed.

3.1. Virtual Engine Model (VEMOD)

The gas dynamics software VEMOD [22] has been used for this study. In VEMOD, the air management is computed by means of a one-dimensional (1D) gas dynamics model that performs the calculations of the flow properties along the intake and exhaust systems as well as the high and low pressure EGR paths. Thus, specific sub-models are considered for the boosting system [23,24], air-charge and EGR coolers, throttle valves, heat transfer including gas-to-wall heat exchange and wall temperature prediction, after-treatment sub-models (DOC and DPF), a 0D turbocharger model, and a hydraulic circuit model. The gas dynamics model is coupled to a cylinder model that predicts the in-cylinder conditions based on the combustion process. Detailed heat transfer model is used to obtain the heat rejection to the chamber walls, while the mechanical losses model allows for obtaining the brake power. An emission sub-model is coupled to the combustion process to predict raw NO_x, CO, HC, and soot emissions as a function of the engine operating conditions. Figure 3 represents the air path systems present in the virtual engine model. Different systems have been remarked in the scheme, such as the intake and exhaust manifolds, the turbocharger, and the high and low pressure paths, as well as the positions of the sensors that send data to the virtual ECU (Engine Control Unit) model.

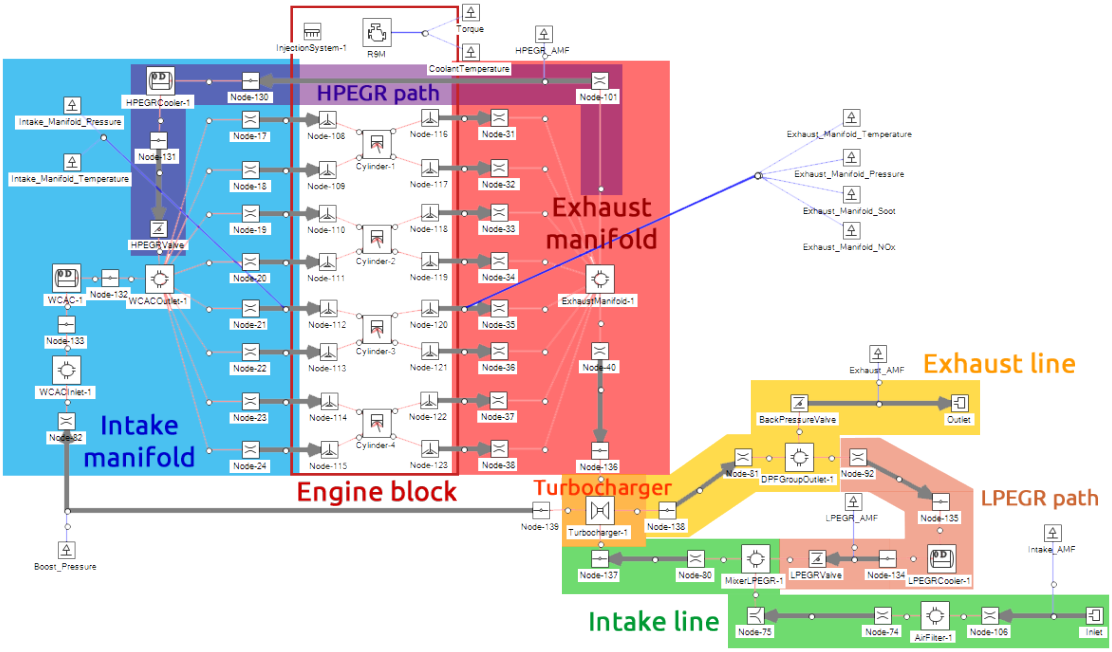

Figure 3. Model scheme of the 1D engine model in VEMOD software.

The turbocharger is based on 0D compressor and turbine sub-models. They use the data that are provided by the supplier maps for both turbine and compressor to compute the flow and the turbomachines efficiencies at any operating point within the maps. Besides, the model is able to extrapolate outside these maps, so it is possible to simulate off-design conditions [25]. The turbocharger sub-model also simulates the heat transfer and the mechanical losses by means of a lumped heat transfer model, hence improving the prediction of the turbine outlet temperature prediction and the heat fluxes that are involved in the turbocharger. A fraction of the exhaust gases energy is not converted into work in the turbine and it is transferred as heat to the ambient, the lubricating oil, and other metal parts of the turbocharger, as depicted from the diagram. Further details of this heat

transfer sub-model and an analysis of the effect of the turbocharger heat and mechanical losses are explained in [26,27].

The combustion and emissions sub-model consists of a 1D model that is able to predict the combustion profile and the main pollutant emissions with an acceptable accuracy. For the sake of completeness, the IMEP relative error is about 3% and the NO_x emissions error is about 8% throughout the Worldwide Harmonized Light-Duty Vehicles Test Cycle (WLTC) [22]. The combustion model is composed of three main sub-models: ignition delay, premix combustion, and diffusion combustion models; along with a 1D model describing the mixing process. A detailed description of the model can be found in [28,29]. The NO_x formation prediction is based on a physicochemical, while, for the other pollutants (soot, CO and UHC), where the fundamentals are unclear and/or that are affected by too many local phenomena, a neural network approach has been developed.

The hydraulic circuits sub-model allows for calculating mass flow and temperatures of oil and coolant at different engine components, like the engine block galleries, the EGR coolers, the turbocharger, and the oil and coolant pumps. Hydraulic circuit elements, like thermostats, operable valves, pumps, and heat exchangers, have been modeled and simulated. The coolant circuit and the oil circuit are based on a thermo-hydraulic network composed of branches, meshes and nodes. By applying the continuity and conservation laws, the mass flows and head losses of the hydraulic networks are calculated. The branches (a pipe between two nodes) are divided into several fluid volumes or parcels in order to calculate the temperature distribution. Simultaneously, the heat exchanger sub-model updates the temperatures. Further details regarding the hydraulics sub-models are collected in [30].

The after-treatment sub-model consists of one DOC model and a DPF model. The DOC model calculates the chemical reactions along the monolith channels, as well as the the mass flow across the device and the outlet gas temperature and canning temperature thanks to a lumped pressure drop model and a heat transfer model. The DPF model, similarly, allow for obtaining the gas mass flow through the monolith as well as its outlet temperature thanks to the pressure and heat transfer models. Soot filtration and regeneration is also considered. Further details regarding the after-treatment sub-model and its calibration procedure are explained in the work that was developed by Payri et al. [21].

Figure 4 shows the flow-chart of the virtual engine model. The blue boxes represent the thermo and fluid dynamics sub-models described above, while the red boxes represent the different control sub-models, which have been developed in Matlab/Simulink. They operate the engine model by actuating over the different actuators that are defined in the engine model. The driver and vehicle model can be detached from the control sub-model if just the engine speed and torque setpoints are provided.

Throughout this study, all of the simulations were performed keeping the torque of the baseline case, which is the one with the original valve timing. A control system included in VEMOD has been used in order to achieve this objective. The control model emulates the ECU to control the injection by modifying the injection pressure, the fuel mass split and the start of injection depending on the engine speed and total fueling rate. The model also controls the air loop by means of the VGT rack position (whose control is based on the intake pressure setpoint, depending on engine speed and total fueling rate), and LP-EGR, HP-EGR, and back pressure valves, where control is based on the air mass flow setpoint. For any specific engine speed and torque, the required fuel mass is obtained from a calibration map. Once the engine speed and fuel mass are known, the injection pulses timings and masses, intake manifold pressure setpoint, injection pressure, and air mass flow setpoints are obtained from their respective maps. These maps were created on the basis of a series of 23 steady-state points spread throughout the entire engine map and using the baseline valve-train configuration.

The calibration process and the results in terms of burn rate, in-cylinder pressure, mechanical losses, pollutant emissions, as well as detailed information regarding the different sub-models are described in [22].

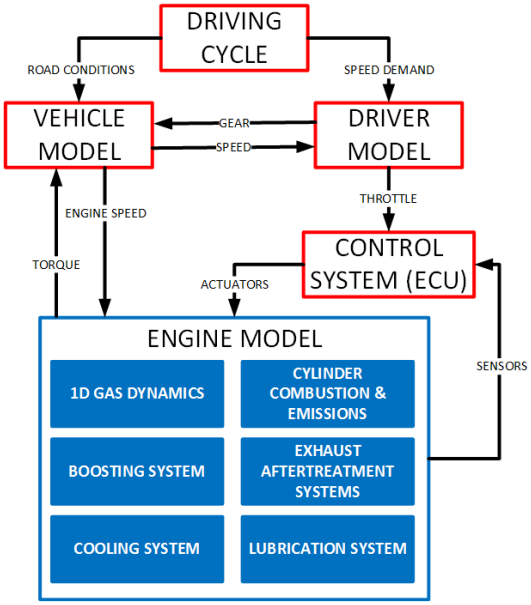

Figure 4. Flow-chart of VEMOD modules.

3.2. Model Validation at Transient Operating Conditions

In Figure 5, several variables are represented comparing experimental measurements versus model results. Figure 5a shows engine brake torque with a coefficient of determination (R^2) of 0.882. This comparison has been done by setting the imposing the experiment fuel mass at each time step of the simulation. The air mass flow target is controlled by the ECU sub-model actuating over the VGT position and the EGR valves. The resulting simulated torque is accurate all along the WLTC.

Figure 5b shows the turbine outlet temperature, which coincides with the gas temperature at DOC inlet. It is interesting to analyze how different VVT strategies affect after-treatment system inlet temperature, particularly during the warm-up time. The faster the light-off temperature (defined as the temperature at which the conversion efficiency reaches 50%) in the catalyst is reached, the faster the efficient oxidation of CO and HC, and the oxidation of NO to NO_2, is achieved. This light-off temperature is considered to be around 200 °C according to an averaged space velocity of 57,700 L/h during the WLTC [9,31]. The decrease in DOC-out NO_2 may have a negative effect on downstream NO_x abatement, specially at temperatures below 250 °C, such as those at engine start up [32]. Moreover, DOC conversion efficiency increases as the temperature grows [21,33], so an increment in DOC inlet temperature may be profitable. The model is able to follow well the turbine outlet temperature trend, specially during the medium and high speed part of the WLTC, where the percent error is below 11%.

Figure 5c shows the coolant temperature at cylinders outlet. In this case, a medium total error of −2 °C along the whole cycle was obtained. Because the coolant temperature has a slight effect on the volumetric efficiency and consumption, and some effect on NO_x formation [34,35], it is interesting to achieve a good prediction. According to the authors, an increase in the coolant temperature leads to an increment of the cylinder wall temperature, which increases the air temperature during the intake stroke, and results in a decrease of the air density. This cylinder wall temperature increment also has some impact on the NO_x formation, especially at low load [35].

Figure 6a,b show NO_x and CO accumulated emissions at engine outlet, right upstream the after-treatment system. NO_x formation is well reproduced along the WLTC. Only at the extra high speed part of the test cycle the NO_x formation is overestimated, with a percent error of 7% at this stage. However, CO formation prediction is underestimated after the low speed part of the WLTC. The CO prediction that is given by the neural network is quite sensitive to small variations in the injection pulses, since the prediction is accurate when the injection timing and mass are those measured on the test bench; contrarily to the current ones, which proceed from the ECU sub-model.

Regarding hydrocarbon emissions, Figure 6c shows a good prediction of total HC at the engine outlet. It can be seen an underestimation at high and extra high speed parts of the cycle. However, the prediction is accurate at the initial stage of the WLTC with a percent error of 8%.

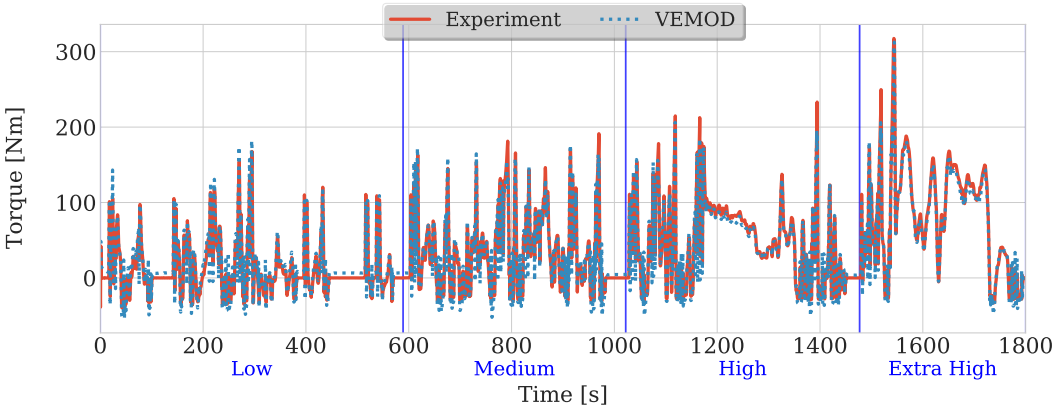

(**a**)

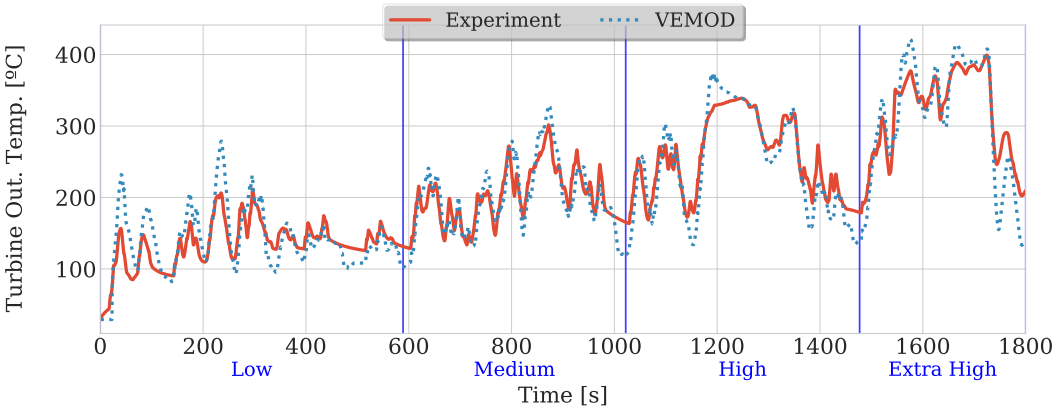

(**b**)

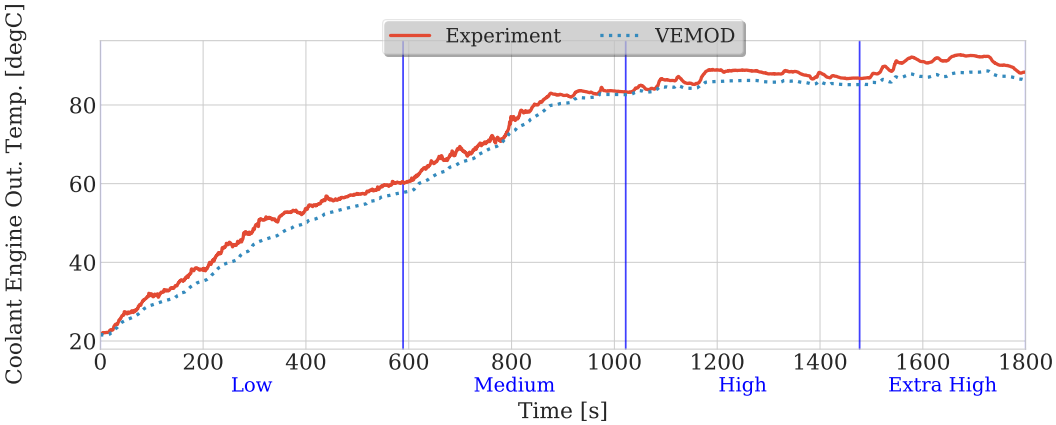

(**c**)

Figure 5. WLTC model validation, engine start at 20 °C room temperature. (**a**) Brake torque; (**b**) EAT inlet temperature; (**c**) Coolant temperature at engine outlet.

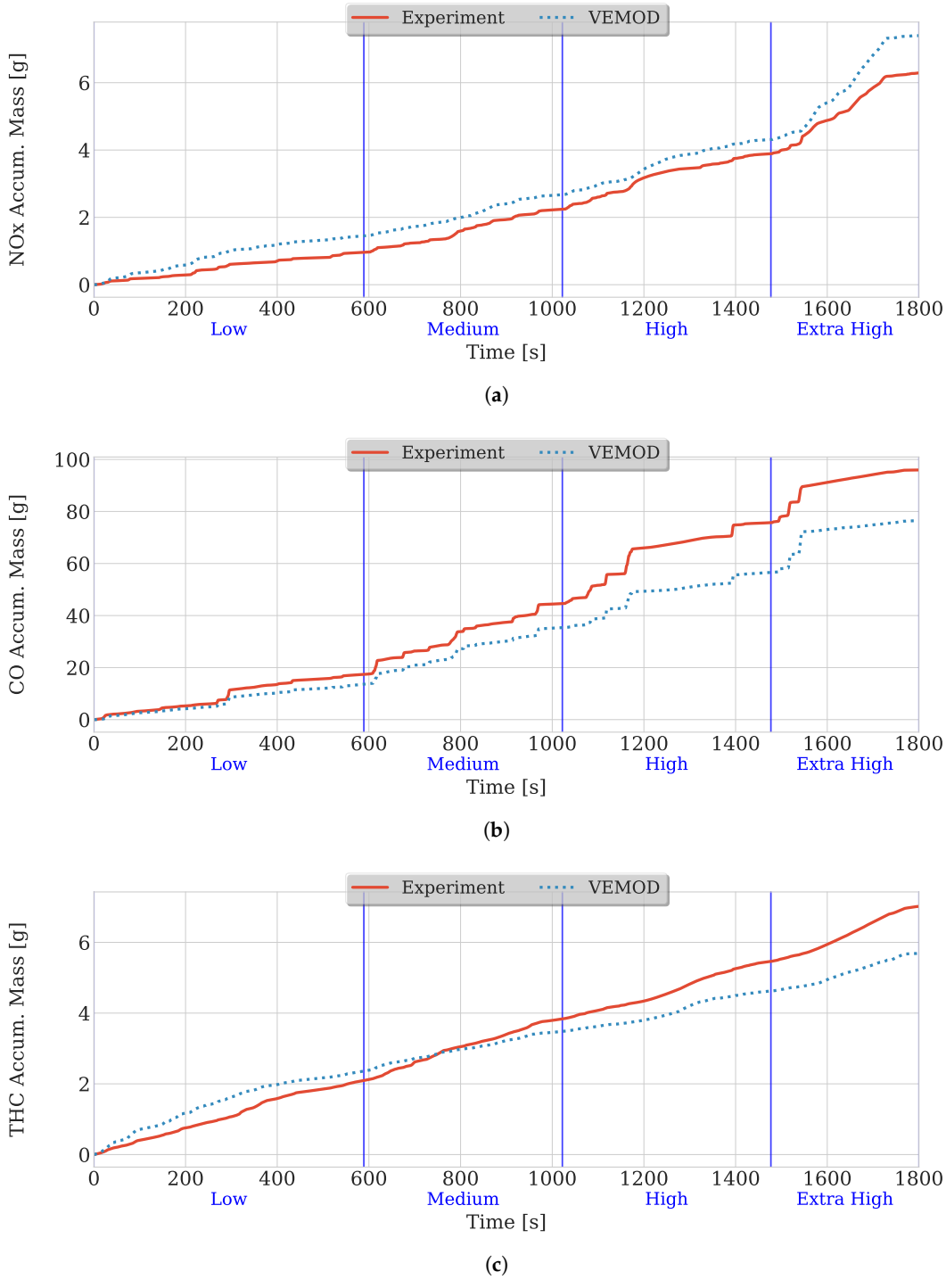

Figure 6. Worldwide Harmonized Light-Duty Vehicles Test Cycle (WLTC) model emissions, engine start at 20 °C room temperature. (**a**) accumulated NO_x mass; (**b**) accumulated CO mass; (**c**) accumulated total hydrocarbons mass.

4. Methodology

This work is centered on how the exhaust temperature can be increased by means of variable valve timing systems. Along this work, three systems have been studied based on a previous work [1]. The first two systems consists in advancing the exhaust event (both EVO and EVC) and, in the same proportion, delaying the intake event (both IVO and IVC). The last systems consist in a second exhaust

opening event (also called re-opening, post-lift, or re-breathing in the literature) during the intake stroke. The aim of these techniques is to raise the exhaust temperature by two different methods that are described below:

- **Exhaust phasing and Intake phasing (EP + IP)**: the exhaust event and the intake event are shifted the same angle, respect to the baseline valve timings. The intake and exhaust valve lifts are represented by a red line with diamond markers in Figure 7. Two versions of this system have been modeled and simulated: one actuating over the cylinder valves and the other actuating only over one intake valve and one exhaust valve. The increase in the exhaust temperature is created, partially, due to the EEVO, since the exhaust blowdown of hot gases from the combustion into the exhaust ports increases the temperature downstream this point. Moreover, some amount of burnt gases are retained later during the intake stroke due to the early EVC, increasing the air-charge temperature at IVC. The late IVO avoids a hot backflow of these burnt gases into the intake manifold, and it compensates the pumping losses due to the compression of these gases with the following brief expansion between TDC and IVO. A parametric study has been done in steady-state conditions by modifying the advance/delay from 10° CA to 80° CA in 10° steps, as seen in Figure 7.
- **Exhaust valve re-opening (EVrO)**: it consists in a second exhaust event during the intake stroke. The intake and exhaust valve lifts are represented by a blue line with triangle markers in Figure 7. The light blue dashed lines represent the minimum and maximum re-opening possibilities. In this case, the re-opening is only applied over one of the exhaust valves and the way it increases the exhaust temperature is by aspiring part of the expelled gases from the exhaust ports back to the cylinder during the intake stroke. In this way, the air-charge temperature at IVC is higher than in the baseline case. A parametric study has been carried out by modifying the re-opening lift from 1 to 5 mm, in steps of 1 mm; re-opening start from 370° CA (just after EVC) to 430° CA, in 10° CA steps; and, re-opening duration from 60° CA to 160° CA, in 20° CA steps, resulting in a three-dimensional (3D) matrix of 210 combinations.

The parametric study has been carried out by simulating each combination of the matrix in steady-state operating conditions. The selected steady-state operating points consists of 23 points trying to cover the full speed-load engine map. These 23 points were tested in the engine test bench and used in the calibration and validation of some of the VEMOD sub-models. These 23 points can be identified in the maps of Figure 8 as black dots.

The simulation of the steady-state operating points was performed by setting the torque and engine speed of the homologous point corresponding to the original valve-train configuration. The ECU sub-model obtains the proper fuel mass for each injection pulse, their start of energizing, and injection pressure from the calibration maps. The model also takes control of the VGT position, the HP and LP-EGR valves and the back-pressure valve to set the boost pressure and the air mass flow. It can increase the injected fuel to meet the torque target; however, there are two fuel limiters: one ensures that the injected fuel do not overpass the one of the full load at that engine speed and the other one limits the fuel to avoid an excess of soot. This translates into the possibility that some of the combinations could not meet the torque demand at any specific operating point. For these reason, all of the combinations have been checked for each of the 23 points, excluding them if the resulting torque is less than a 5% lower of the baseline in that specific operating point.

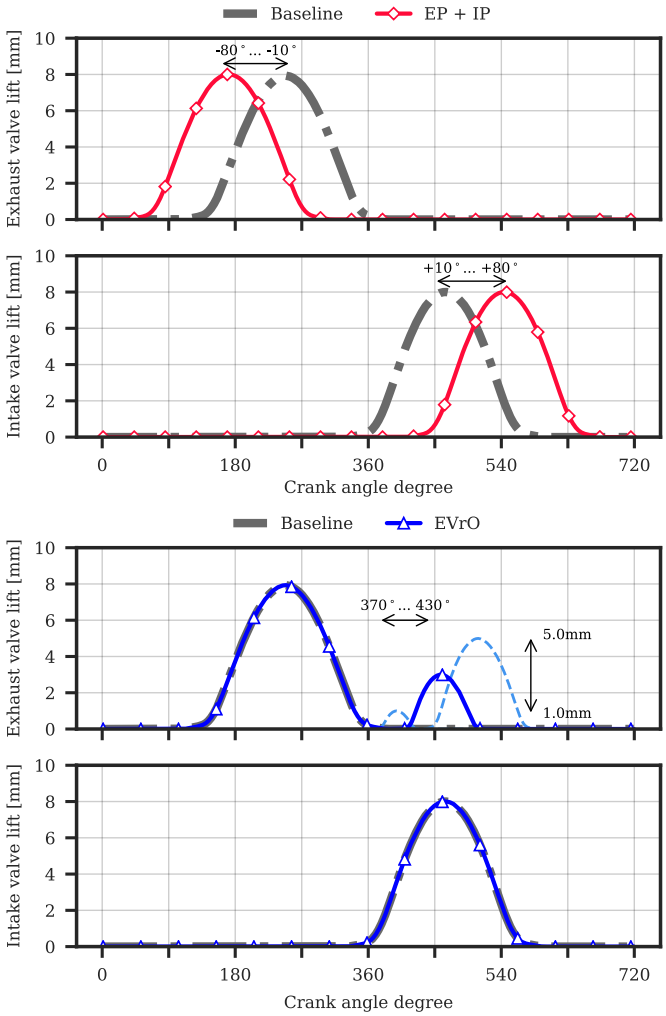

Figure 7. Exhaust and intake valve lift profiles for each case.

With all of the information gathered from the parametric study, it is possible to state objectives and select those combinations that meet the objective for each steady-state operating point. For this study, five different cases have been defined with the aim of achieve the higher exhaust temperature. This five cases, plus the baseline, are summarized in Table 3. One case corresponds to the "EP + IP" alternative applied on the four cylinder valves. Two cases (Cases 2 and 3) considers the "EP + IP" alternative, but applied on one intake valve and one exhaust valve. The two cases left corresponds to the goal of maximize DOC inlet gas temperature by performing an exhaust re-opening. Cases 3 and 5 represents Cases 2 and 4, respectively, but imposing a maximum fuel penalty of 10% with respect to the baseline.

Table 3. Transient cases.

Case	Technology	Objective
Baseline	Original valve timing	-
Case 1	EP + IP in the 4 valves	Maximize DOC inlet temperature
Case 2	EP + IP in only 2 valves	Maximize DOC inlet temperature
Case 3	EP + IP in only 2 valves	Maximize DOC inlet temperature, limiting the fuel penalty up to 10%
Case 4	EVrO in only 2 valves	Maximize DOC inlet temperature
Case 5	EVrO in only 2 valves	Maximize DOC inlet temperature, limiting the fuel penalty up to 10%

EP + IP: Exhaust negative phasing and intake positive phasing, EVrO: Exhaust valve re-opening.

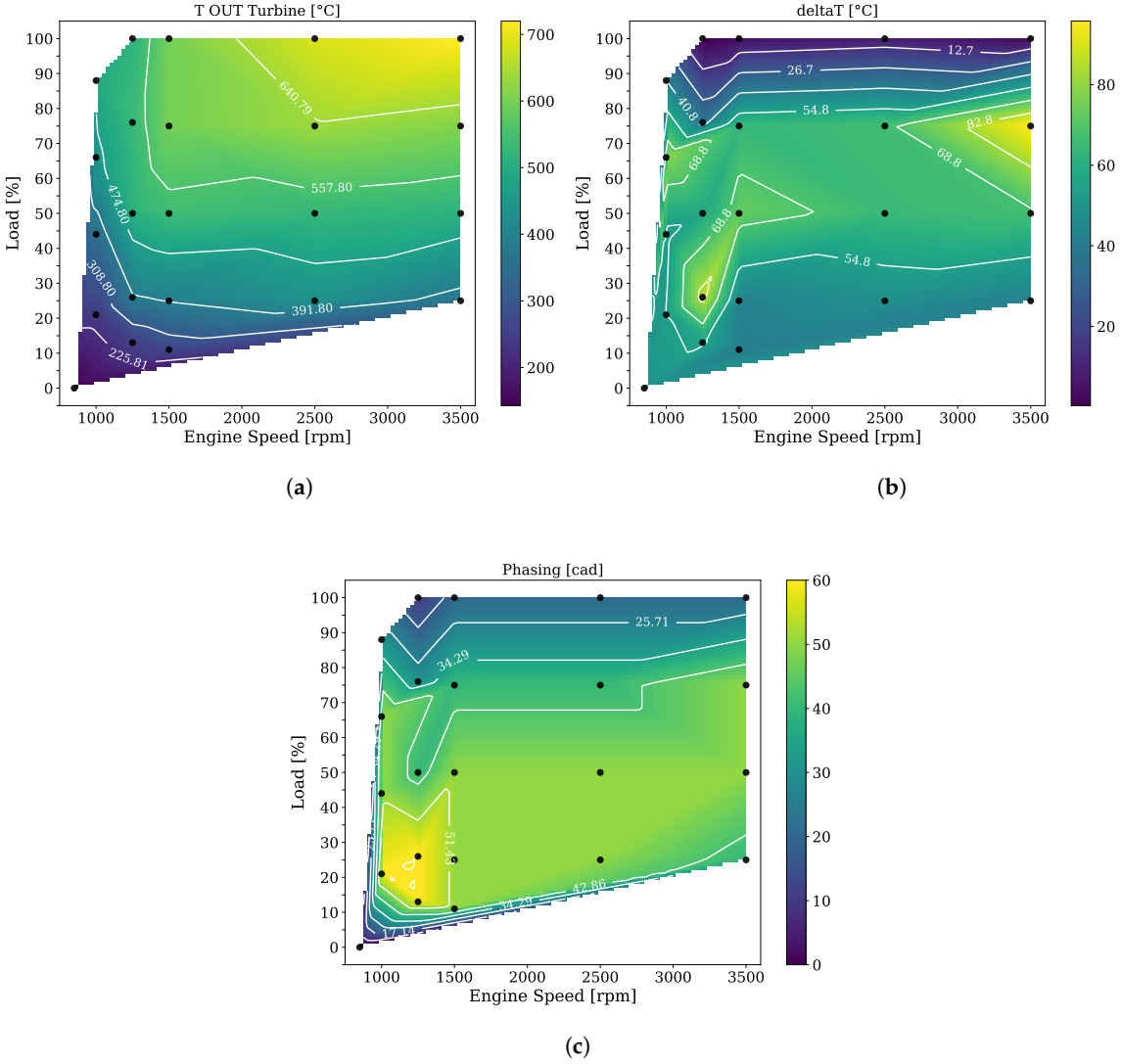

Figure 8. Temperature at turbine outlet and valve phasing maps for Case 3. (**a**) Temperature map at turbine outlet.; (**b**) Temperature difference map at turbine outlet respect to the baseline case; (**c**) Valve phasing map.

An "EP + IP" control (intake delay and exhaust advance) and an "EVrO" control (start, duration, and lift) were included in the ECU sub-model in order to carry out the transient simulations. This controllers read the current value of re-opening lift, start, etc., from a map like the one on Figure 8c, based on the current engine speed and torque. For each case defined in Table 3, a set of maps must be created. For instance, Figure 8a shows the gas temperature map at turbine outlet in Case 3. Figure 8b shows this same temperature as a difference between the baseline case. An increase of more than 50 °C can be reached up to 80% load at any engine speed. Finally, Figure 8c represents the angle phasing map in Case 3. It can be observed that a phasing of 40° CA is applied above idle to 70% load.

Finally, the WLTC cycle from cold engine start, at a room temperature of 20 °C, is simulated keeping the settings of each case and using their respective maps for "EP + IP" phasing or "EVrO" start, duration and lift.

5. Results and Discussion

The main goal of this study is to achieve greater exhaust temperatures in order to increase the efficiency of the after-treatment devices during their heating phase. In Figure 9, the temperature at the turbine outlet section, intermediately preceding the catalyst, achieved by each case is presented.

It can be observed that this temperature is higher than the baseline in the five cases throughout the whole WLTC. This temperature difference can be better observed in the lower subplot. At the low speed stage, both "EVrO" cases do not offer a remarkable difference in the temperature increment. Comparing the three "EP + IP" cases, Case 2 performs better during this low speed stage than Case 1, achieving instantaneous peak differences higher than 100 °C and an average difference at this stage of 67 °C. From the medium speed stage onwards, both "EVrO" cases perform better than Case 3. This means that, with the same limitation in fuel consumption, Case 5 is able to obtain more exhaust temperature than Case 3. Case 1, in which the intake and exhaust phasing is applied on the four valves, generally performs worse than the two valves case. The average temperature difference in Case 1 is 98 °C throughout the whole WLTC, in contrast to the 121 °C achieved by Case 2.

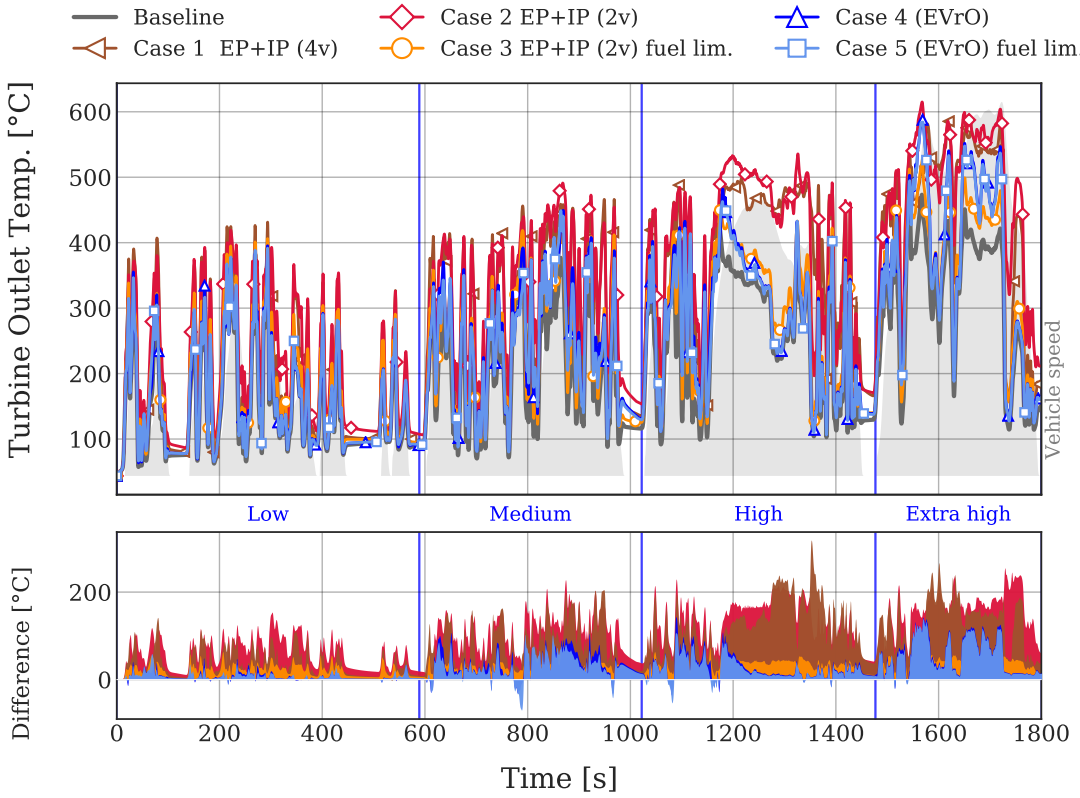

Figure 9. Worldwide Harmonized Light-Duty Vehicles Test Cycle (WLTC) temperature at turbine outlet.

Figure 10 shows how much time the temperature at the turbine outlet section is above a certain value. The minimum temperature values (the initial ones) are shown at the top of the graph, since, for the total test time (1800 s), the temperature is above this minimum values. The maximum values are shown in the bottom of the graph because they are only achieved at one instant. Maximum values are also indicated in the legend. It can be observed that all the Cases allow for reaching higher temperatures than the baseline valve-train. Both "EVrO" Cases and Case 3 show a similar behavior for around 1600 s. Cases 4 and 5 achieve higher temperatures than Case 3 for 200 s, which correspond to the final high speed accelerations of the WLTC. Case 2 depicts the higher temperature of all cases and Case 1 performs in between of Cases 2 and 3. If vertical line is drawn between 200 °C and 250 °C, where the DOC conversion efficiency surpasses 50%, the temperature of the baseline case will be above this value for 800 s. In Cases 3–5, this time is extended up to 900–950 s. Case 2 is able to keep a temperature above this level for 1150 s.

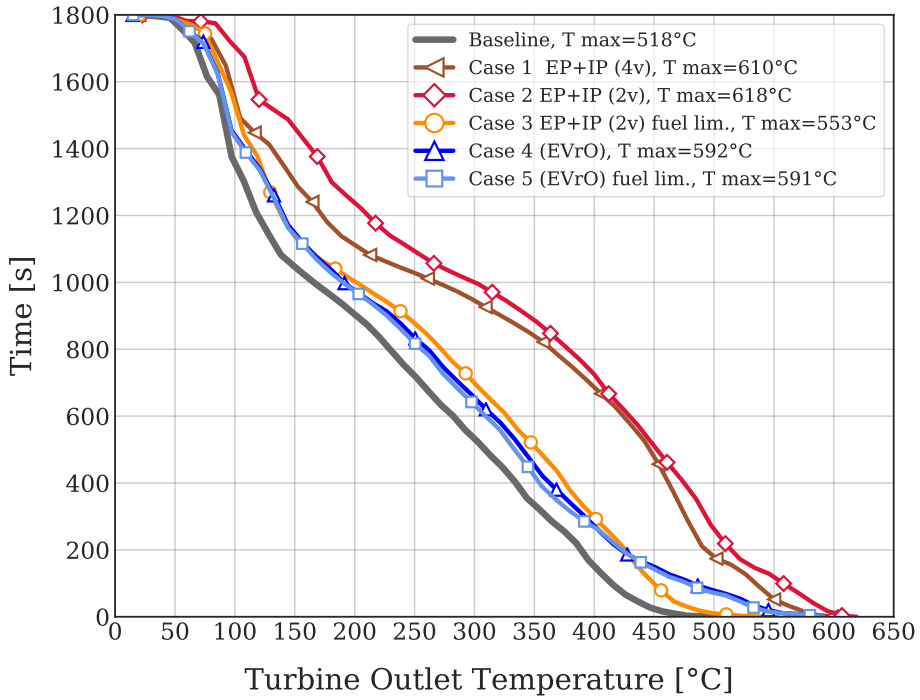

Figure 10. Time above a certain temperature at turbine outlet.

In addition to the DOC inlet temperature, it is also interesting to analyze how the different cases affect the gases temperature at DOC outlet section. A temperature increment at this point could be profitable for increasing the efficiency of a NO_x adsorber, or to regenerate the Diesel particle filter. Figure 11 shows the gas temperature downstream the DOC, before entering the DPF. Similarly to Figure 9, "EP + IP" cases perform better than "EVrO" ones and Case 2 achieves the greatest increment in temperature. Its average increment throughout the test cycle is 80 °C, followed by case 1, with an average of 53 °C. It is also noticeable how Case 4 and Case 5 obtain less temperature than the baseline case at some moments, like the one near 800 s. At this time, the engine is accelerating from 1000 rpm to 1250 rpm at a low torque. According to the re-opening lift map that was obtained by the steady-state optimization, the relatively high lift value in this region of the map causes a torque fall down in transient operating conditions.

Figures 12 and 13 represent the HC and CO accumulated conversion efficiencies in the DOC, respectively, and calculated according to Equation (1) (where Pollutant can be either HC or CO, and i refers to the current timestep). As commented above, a higher gas temperature across the DOC increases HC and CO conversion efficiencies. Regarding HC conversion, Case 2 is able to increase the conversion efficiency an 8.5% during the low speed stage, respect to the baseline case, being able to reach an efficiency of 0.97. In other words, Case 2 is able to remove the 98% of the inbound HC. Case 1 increases the HC conversion a 4% during the first stage, far enough of "EVrO" cases which improves slightly the conversion of the baseline. At the end of the cycle, the accumulated HC conversion efficiency of Case 2 drops down, since the HC formation increases during the extra high speed stage due to its fuel penalty, when compared to the baseline case. The same effect is observable for Case 3. Contrarily, the accumulated conversion in Case 1 ("EP + IP" applied on both pair of valves) continuously increases to reach a final value of 0.98.

$$Pollutant\ Accum.efficiency_i = \frac{(\sum_{i=1}^{n} Pollutant\ mass_i)_{inlet} - (\sum_{i=1}^{n} Pollutant\ mass_i)_{outlet}}{(\sum_{i=1}^{n} Pollutant\ mass_i)_{inlet}} \quad (1)$$

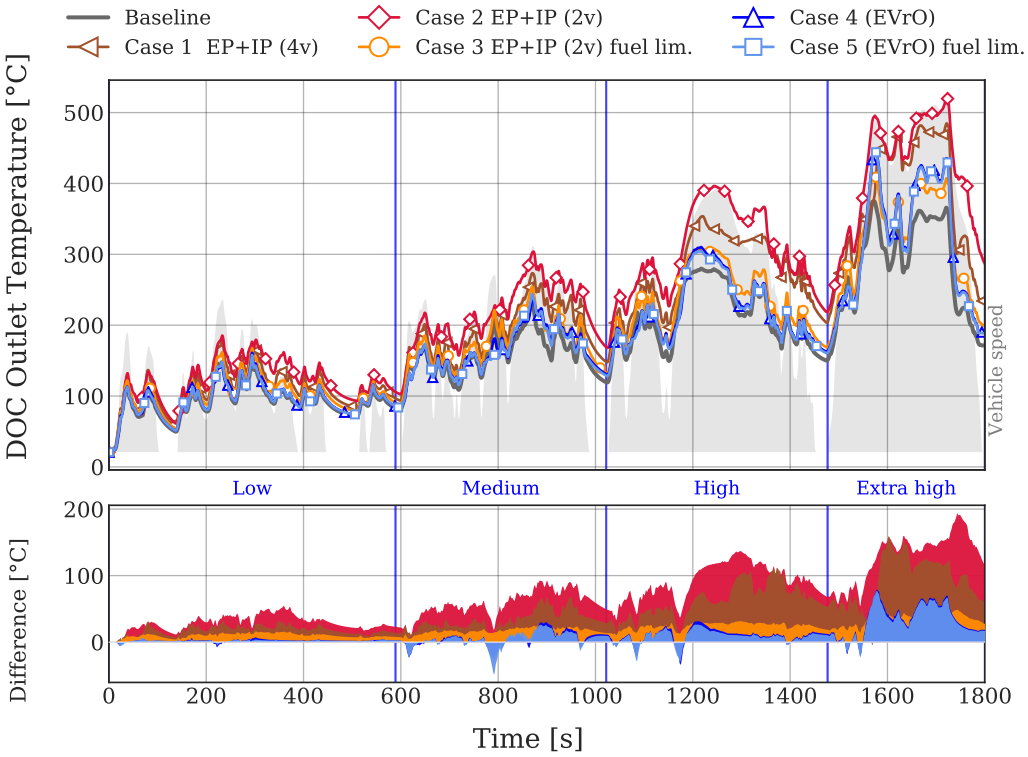

Figure 11. WLTC DOC outlet temperature.

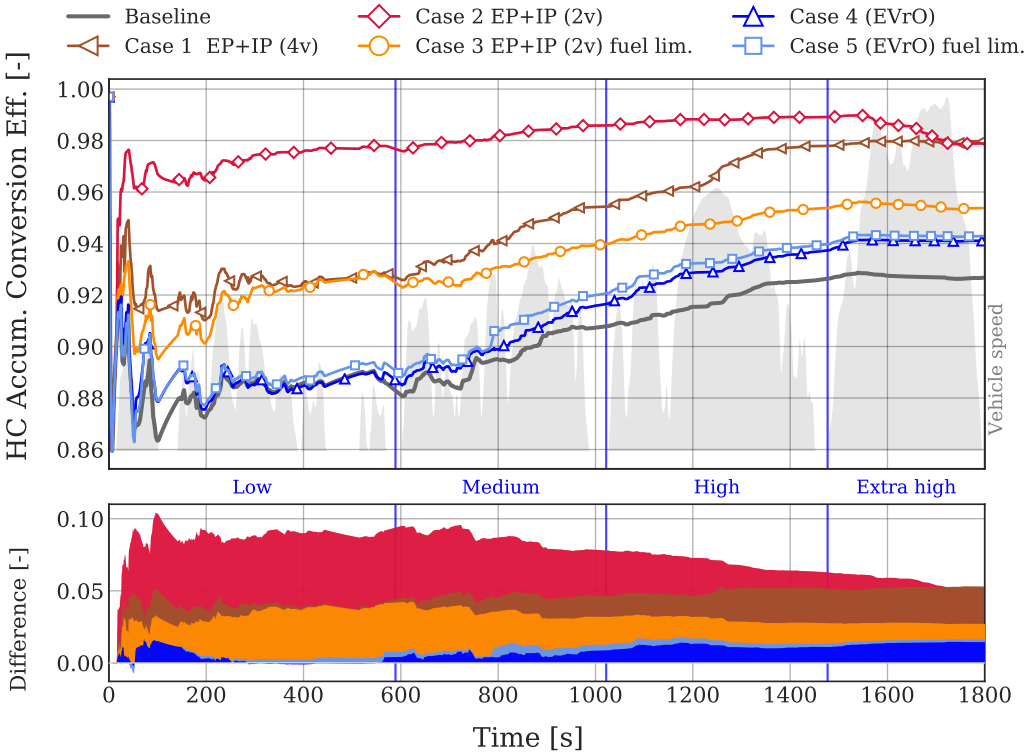

Figure 12. WLTC HC accumulated conversion efficiency.

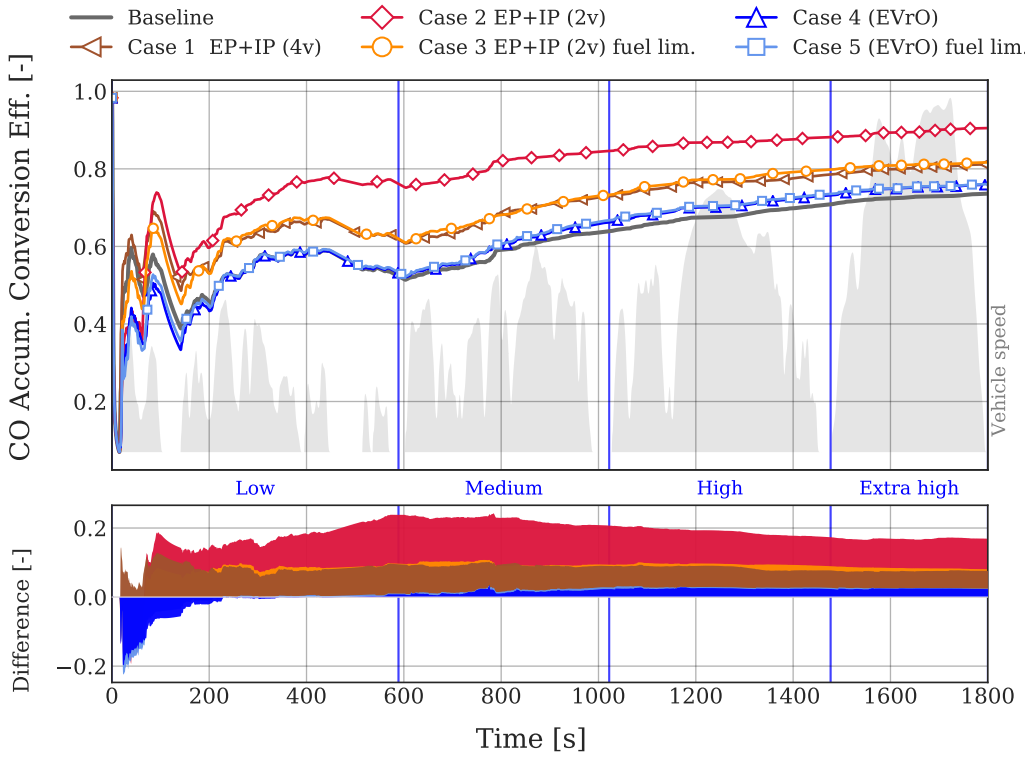

Figure 13. WLTC CO accumulated conversion efficiency.

A similar trend is observable with respect to CO accumulated conversion efficiency in Figure 13. It is noticeable how the CO conversion of Cases 4 and 5 is lower than in the baseline, this is not due to an increment in CO formation but with the inability to reduce DOC outbound CO emissions due to a lower exhaust enthalpy compared to the baseline case. From the second idle period of the cycle onwards, "EVrO" cases reflect a minor improvement in CO conversion. Case 1 reaches the higher CO conversion efficiency due to its highest temperature increment, with an average increment of 18%. However, as it happened with the HC conversion, it falls down by the end of the WLTC due to the fuel penalty of "EP + IP" at high load. This effect is less evident in Case 3, where the maximum fuel penalty is limited to 10%.

In terms of NO_x formation, Figure 14 shows how there are no important differences until the high speed stage of the WLTC. During the fast accelerations at high engine speed, Cases 1 and 3 produce a higher amount of IGR than "EVrO" cases. Thus, reducing NO_x formation at high engine speed. Cases 4 and 5, on the contrary, do not perform so well in terms of exhaust gases retention. This, plus the fact that the air loop controller closes the LP-EGR valve more than in the baseline case, leads to greater NO_x formation, which can be observed better in the bottom subplot of Figure 14. The accumulated differences of NO_x emissions are later described in relative terms in Figure 15d, which they are separated into emissions at the end of the low speed stage and emissions at the end of the full WLTC.

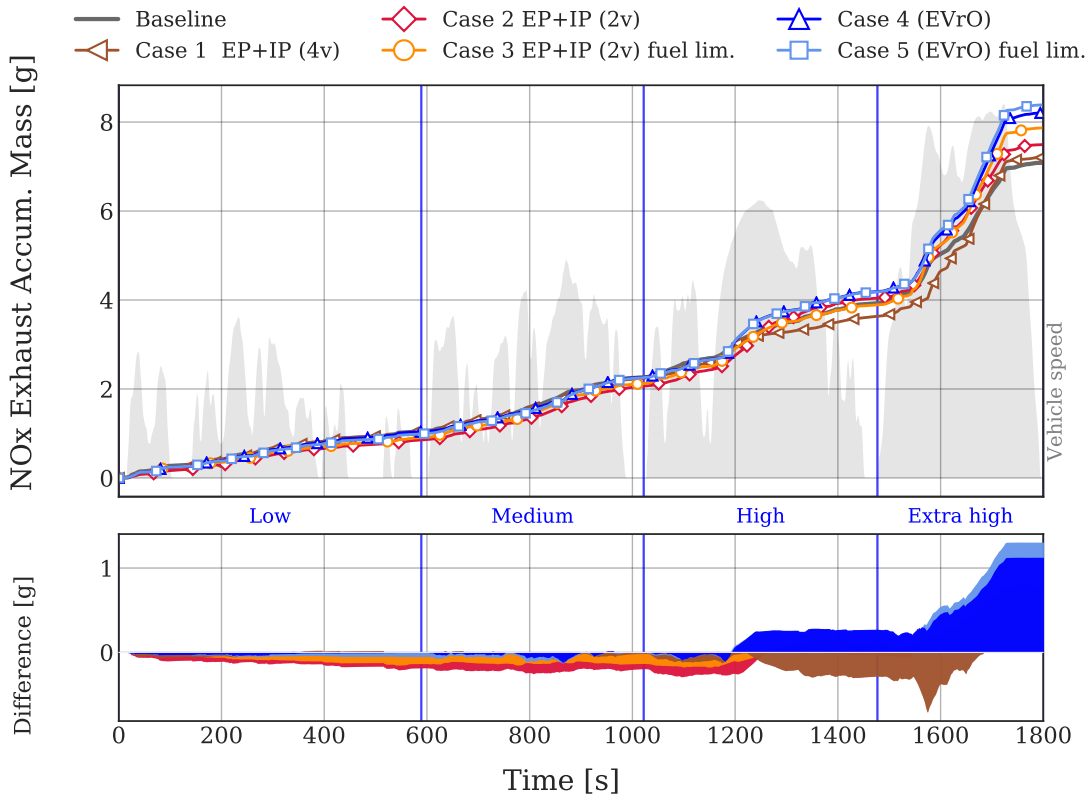

Figure 14. WLTC NO_x accumulated mass.

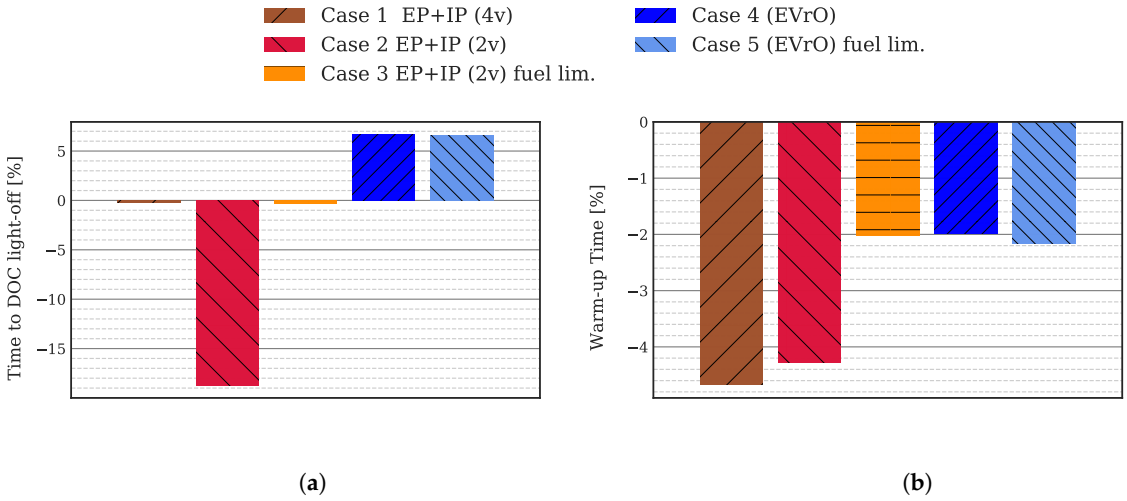

(**a**) (**b**)

Figure 15. *Cont.*

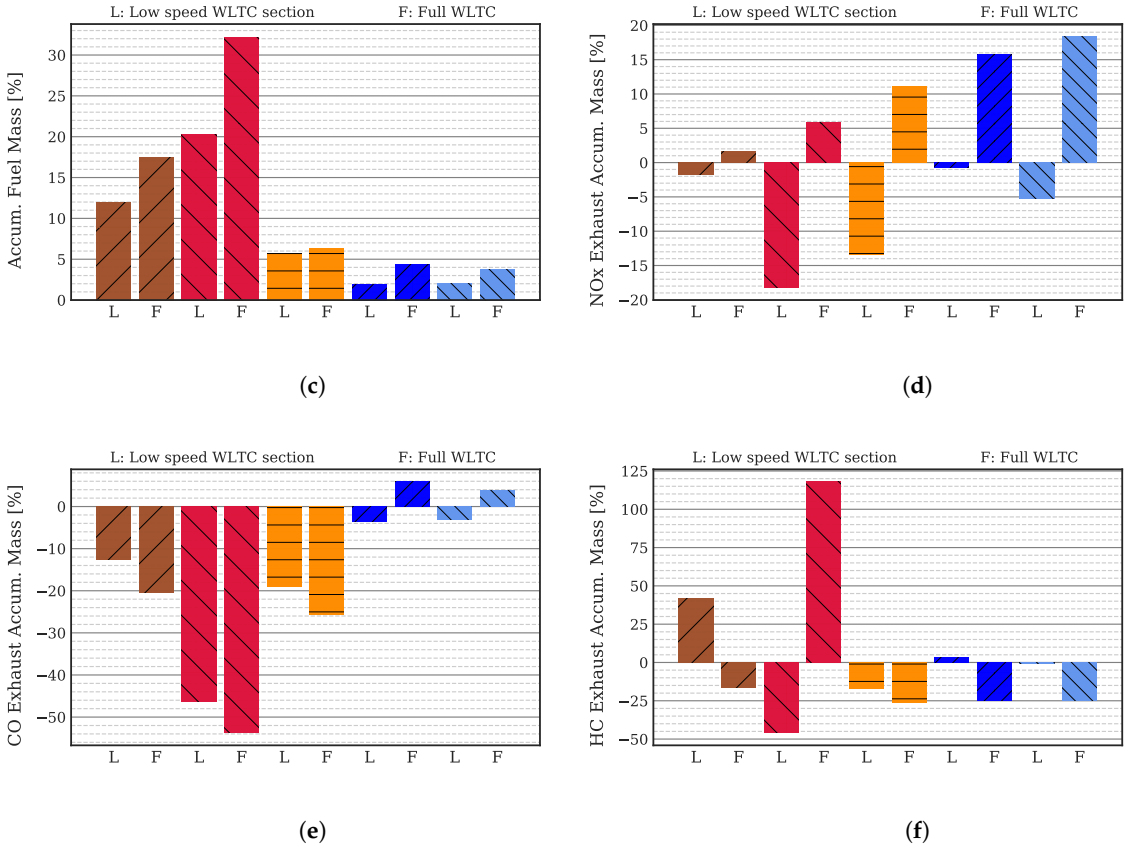

Figure 15. WLTC model results during the low speed stage and the whole cycle, engine start at 20 °C ambient temperature. Percentage variation compared to the baseline case. (**a**) Time to reach DOC light-off temperature; (**b**) Time to reach coolant thermostat threshold; (**c**) Accumulated fuel consumption; (**d**) Accumulated engine-out NO_x emissions; (**e**) Accumulated CO emissions at DOC outlet; (**f**) Accumulated HC emissions at DOC outlet.

The set of graphs in Figure 15 displays some interesting values regarding the performance and emissions of each case in transient operating conditions. Each case is represented by two bars, except for the light-off time and warm-up time. The first bar indicates the accumulated value variation, with respect to the baseline case, at the end of the low speed stage (L) of the WLTC (at 589 s); whilst the second bar indicates the final accumulated value variation (F). In terms of DOC activation (Figure 15a), as it was shown before, Case 2 allows for obtaining the greatest temperature in the DOC temperature, so the DOC light-off is achieved a 18.7% sooner (around 150 s before the baseline). Cases 1 and 3 cannot reduce the light-off time, since they do not reach at least 200 °C in the previous accelerations. Regarding Cases 4 and 5, their delay in the light-off time (a 6.6% later) is due to the slight lack of power in the preceding acceleration near 800 s; otherwise, there would be no difference between Cases 1, 3–5.

Warm-up time is defined as the time that it takes for the coolant to reach a certain temperature, which is around 80 °C in this particular engine, and the thermostat valve starts to funnel the coolant flow through the radiator cooler to stabilize its temperature. Moreover, the coolant temperature plays an important role in this engine, since it controls the switch between HP-EGR to LP-EGR. The warm-up stage can be shortened in all cases, being Cases 1 and 2 the ones that present a higher reduction of 4.7 and 4.3%, respectively, as can be observed in Figure 15b. The higher temperature in the exhausts ports results in a heating of the coolant that surrounds these ports and, hence, reducing the warm-up time.

In terms of fuel consumption in Figure 15c, it can be observed how the three "EP + IP" cases incur in a fuel penalty higher than the one of both "EVrO" cases. The higher fuel consumption as compared to the re-opening cases is due to the compression of the retained burned gases after the EVC, since this compression increases the pumping losses and, thus, the BSFC. The earlier EVO also affects

fuel economy as it reduces the power stroke and increases the amount of fuel injected to keep the required torque. This fuel penalty increases with the engine load, as it can be seen by the accumulated values at the end of the WLTC. Case 2, while offering the highest exhaust temperature increment, incurs in the highest fuel penalty with a total difference of 32.2% (340 g more than the baseline). Case 3 offers a better solution in fuel economy, as it is a version of Case 2, in which fuel injected has been limited. On the other side, both Case 4 and 5 do not affect fuel economy in the same way. Their total accumulated fuel burned variations are 4.4% (+46 g) and 3.8% (+39 g), respectively.

Regarding NO_x emissions, it is observed an increase in all cases at the end of the cycle. When it comes to "EP + IP" cases, and upward trend is observed in NO_x formation as engine speed increases; since the accumulated values during the low speed stage are lower than in the baseline but higher at the end of the cycle. The increase in NO_x formation when compared to the baseline case can be explained because of the lower EGR mass flow when increasing the engine speed. In the extra high speed stage of the WLTC, the air loop controller closes the LP-EGR valve in all cases more than in the baseline one. However, when considering the CO_2 mass fraction at IVC, both "EVrO" cases show a lower exhaust gas retention power at high speed. Thereby, the NO_x formation is higher in Cases 4 and 5 during this last stage. An 18.2% reduction in NO_x formation can be obtained in Case 2 over the low speed stage of the WLTC. Analyzing NO_x emissions when performing an exhaust re-opening it can be observed that emission levels are higher in both cases. Exhaust NO_x emissions increase with the engine speed, as the amount of IGR created by the re-opening is lower at high engine speed, leading to a final increase of 18.4% in Case 5, with respect to the baseline in case.

Figure 15e shows the CO accumulated mass downstream the Diesel catalyst. Even though performing an exhaust re-opening does not affect the CO formation (specially at low engine speed), the poor potential in order to heat the catalyst leads to CO emission levels that are higher than those achieved by the "EP + IP" cases. Case 2 is the most profitable in this with respect with a reduction 46.4% at the end of the low speed stage and a 53.7% reduction over the full cycle, when compared to the baseline case.

As regards HC emissions downstream the DOC, Figure 15f depicts that Cases 2 and 3 improve HC emissions during the low speed stage of the cycle. However, in Case 2, due to the high fuel penalty during the extra high speed stage, the final HC emissions double the baseline ones (an increase of 117%). This is also observable in Figure 12, where there is a decrease in the accumulated HC conversion efficiency. Case 4 and 5 are able to reduce HC emissions down to a 25% at the end of the cycle due to their contribution in the DOC gas enthalpy while not incurring in an excessive fuel penalty at the high speed stage.

Figure 16 represents some trade-offs between engine consumption and CO and HC emissions only during the low speed stage of the WLTC. Emissions inbound the DOC are shown on the left side, while emissions outbound the DOC are placed on the right side. It can be seen that Cases 1–3 increase the CO formation (Figure 16a). The greater values are explained due to the fact that performing an EEVO results in an increase in fuel injected mass, which leads to an increment in HC and CO. Moreover, the earlier blowdown interrupts the oxidation of HC and CO during the expansion stroke. The fuel consumption difference between Cases 1 and 2 ("EP + IP" in 4 v vs in 2 v) is because, when phasing both pair of valves, it is difficult to keep the target torque with high EEVO and LIVO angles. In case of phasing just one intake valve and one exhaust valve, the phasing range is wider. However, extending this range leads to a higher fuel consumption in Case 2, which is 20% more than the baseline. In Figure 16b, it can be seen how the excess in CO formation of "EP + IP" cases is later compensated by the increase in CO conversion. Accordingly, Case 3 offers a good trade-off between fuel penalty and CO emissions, being able to reduce them by a 20% with a fuel penalty of 6%.

Figure 16c,d presents similar trends to CO pollutant emissions. The fuel penalty caused by advancing EVO moment increases HC emissions. This consumption increase is almost directly proportional to the exhaust temperature increase. Figure 16d shows how the HC formation in Cases 2 and 3 are later compensated by the increment in the HC conversion efficiency. Nonetheless,

Case 1 is unable to reduce total HC emissions at the end of the low speed stage. Even though the reduction between inlet and outlet emissions is near 71%, higher than the reduction in Case 3 (51%), the hydrocarbons formed over the combustion are higher when compared to Cases 3–5.

It is interesting to note that the fuel that is consumed by Cases 4 and 5 is pretty much the same. In fact, the difference in fuel consumption, as compared to the baseline case, across the engine map is below 10% for a wide region of that. Case 5 just ensures that it does not exceed a fuel penalty of 10% in any region of the fuel map.

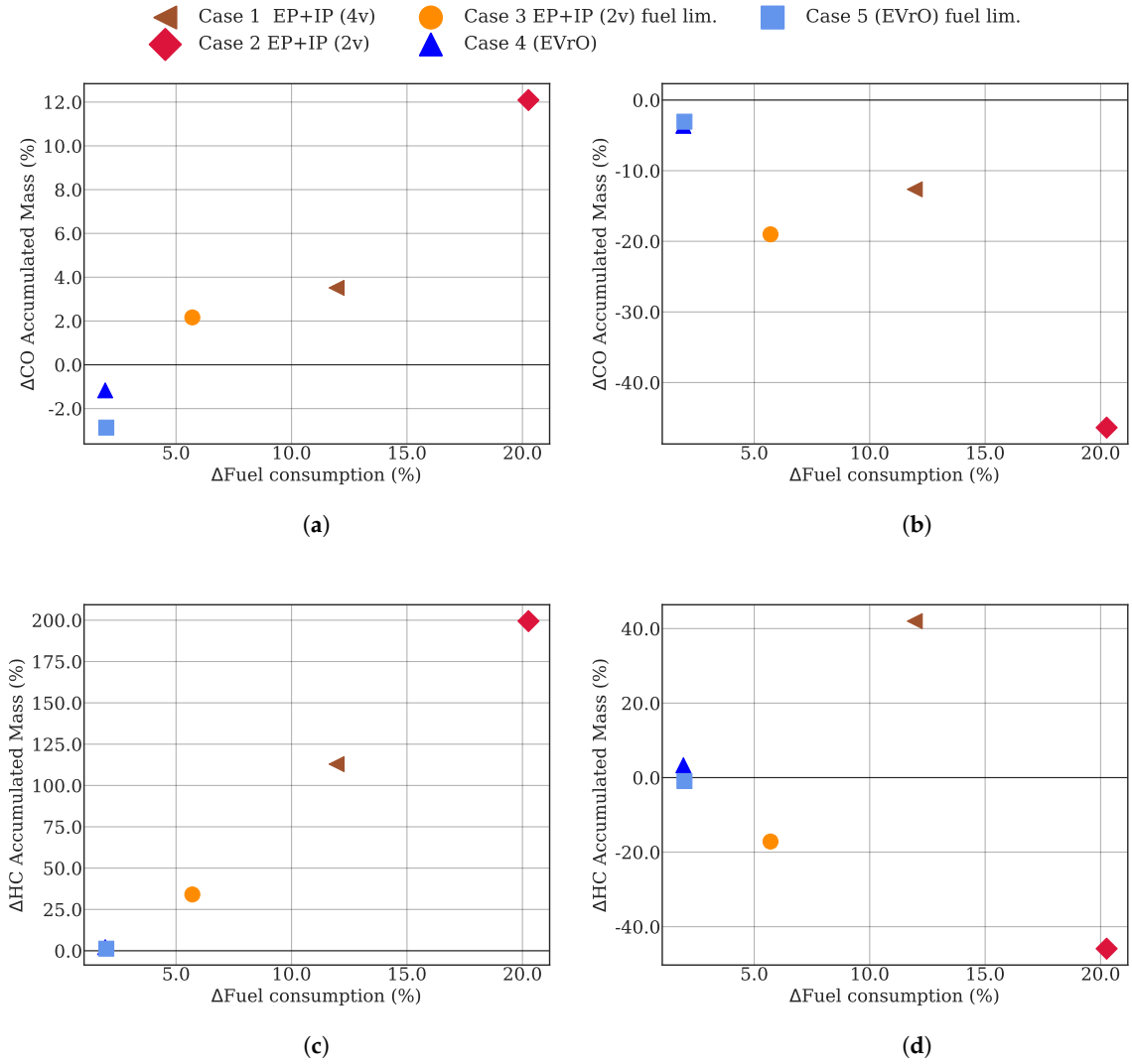

Figure 16. Fuel consumption variation (%) versus CO and HC accumulated mass variation (%) trade-offs during the low speed stage of the WLTC, taking the baseline case as the reference. (**a**) Fuel consumption (%) versus CO accumulated mass (%) upstream the DOC. (**b**) Fuel consumption (%) versus CO accumulated mass (%) downstream the DOC. (**c**) Fuel consumption (%) versus HC accumulated mass (%) upstream the DOC. (**d**) Fuel consumption (%) versus HC accumulated mass (%) downstream the DOC.

6. Summary and Conclusions

Several variable valve timing alternatives have been discussed in this work with the aim of improving the temperature upstream de Diesel catalyst. Three types of variable valve solutions have been studied based on previous studies [1]: advancing EVO and EVC, with a symmetrical delay in IVO and IVC, on one and on both pairs of cylinder valves; and, a exhaust valve re-opening during the

intake stroke. In order to operate with optimum values of intake/exhaust phasing, and re-opening lift and duration, a control system has been integrated to the ECU sub-model. These values were obtained by means of a parametric study in steady-state operating conditions. With the proper "EP + IP" and re-opening maps for each case, a simulation of the WLTC cycle starting at cold start at 20 °C was carried out for each case. These five cases have been compared in terms of exhaust temperature profit, fuel consumption, warm-up and light-off time, and pollutant emissions. For the sake of summarizing the conclusions obtained, the following points are exposed:

1. The exhaust temperature is increased and the warm-up time reduced in all the five cases. The increase in the exhaust gas temperature allows higher CO and HC conversion efficiencies in the catalyst. "EP + IP" cases are the most profitable in this way. Case 2 achieves an average increment in exhaust temperature of 67 °C, followed by Case 1 with an average increase of 42 °C over the low speed stage. Case 2 allows the greatest increment in HC and CO accumulated conversion efficiency: 8.5% more than the baseline, for HC conversion, and 18% for the CO over the low speed stage of the WLTC.
2. "EVrO" alternatives (Cases 4 and 5) do not offer a noticeable increase in the exhaust temperature over the low speed stage of the test cycle, compared to the other cases. Their average increase over this stage of the WLTC is around 8 °C.
3. Cases 4 and 5 can reduce slightly the CO and HC formation. However, they cannot reduce the tailpipe emissions as much as Cases 1–3 (specially over the low speed stage) due to their low contribution towards increasing the exhaust gases enthalpy. At the end of the low speed stage of the WLTC, HC and CO accumulated conversion efficiencies of both "EVrO" cases are fairly similar as the baseline ones.
4. Despite the high temperature increase offered by Case 2, its accumulated fuel penalty reaches a 20% at the end of the low speed stage; and it is even higher during the extra high speed. In terms of fuel consumption and emission trade-off, Case 3 arises as a good alternative to reduce HC and CO emissions and provide an increase in the tailpipe temperature, which is profitable for NO_x adsorbers placed downstream the DOC.
5. Regarding NO_x formation, Cases 2 and 3 allow to obtain a slight reduction in absolute values during the low speed stage of the WLTC, reducing NO_x emissions by 18% and 13%, respectively. On the contrary, the maximum excess in NO_x is near 16%, which is reached by Case 5 over the last high speed transients of the WLTC. "EVrO" strategies (Cases 4 and 5) do not achieve the same exhaust gas retention power as the other cases for the fast accelerations during the extra high speed stage.
6. Regarding "EP + IP" cases, when the phasing is applied on the four valves, rather than on two valves, the phasing range gets reduced in order to keep the torque target. Nonetheless, a high advance of the EVO, like in Cases 1 and 2, drastically increases the fuel consumption. The fuel penalty in Case 1 is about 12%, while the one of Case 2 is about 20% at the end of the low speed stage.

As a concluding remark, Case 3 presents the best CO-fuel and HC-fuel trade-offs. Moreover, it is possible to achieve an 18% reduction in NO_x emissions following this strategy during the low speed stage of the WLTC. Its accumulated fuel consumption is about 5% more than the baseline case, which is the lowest of all three "EP + IP" strategies. The main caveat of Case 3 is that, even though it increases HC and CO conversion efficiencies, it is unable to reduce light-off time as much as Case 2. A better alternative would be a mix of Case 2 and Case 3: trying to heat-up quickly the after-treatment system while constraining the fuel penalty, and then switching off the strategy or moving towards a more limitation in the fuel consumption (like in Case 3) once the DOC is already active.

Author Contributions: Conceptualization, F.J.A. and Á.A.; methodology, Á.A. and F.J.A.; software, F.J.A. and J.M.; validation, F.J.A., J.M. and Á.A.; writing—original draft preparation, Á.A.; writing—review and editing, J.R.S., F.J.A. and J.M.; visualization, Á.A.; supervision, J.R.S. and F.J.A.; project administration, J.M. and F.J.A.; funding acquisition, J.M. All authors have read and agreed to the published version of the manuscript.

Funding: This research has been partially funded by the Spanish government under the grant agreement TRA2017-89894-R ("Mecoem"). Ángel Auñón was supported through the "Apoyo para la investigación y Desarrollo (PAID)" grant for doctoral studies (FPI S2 2018 1048) by Universitat Politècnica de València.

Conflicts of Interest: The authors declare no conflict of interest.

Abbreviations

The following abbreviations are used in this manuscript:

0D	Zero-dimensional
1D	One-dimensional
BDC	Bottom Dead Centre
BSFC	Brake Specific Fuel Consumption
CA	Crank Angle
CI	Compression Ignited
CO	Carbon monoxide
DOC	Diesel Oxidation Catalyst
DPF	Diesel Particle Filter
ECU	Engine Control Unit
EEVC	Early Exhaust Valve Closing
EEVO	Early Exhaust Valve Opening
EGR	Exhaust Gas Recirculation
EIVC	Early Intake Valve Closing
EIVO	Early Intake Valve Opening
EP	Exhaust Phasing
EVC	Exhaust Valve Closing
EVO	Exhaust Valve Opening
EVrO	Exhaust Valve re-Opening
FS	Full Scale
HC	Hydrocarbons
HP-EGR	High Pressure EGR
HSDI	High Speed Direct Injection
IGR	Internal Gas Recirculation
IP	Intake Phasing
IVC	Intake Valve Closing
IVO	Intake Valve Opening
LEVC	Late Exhaust Valve Closing
LEVO	Late Exhaust Valve Opening
LIVC	Late Intake Valve Closing
LIVO	Late Intake Valve Opening
LP-EGR	Low Pressure EGR
NO_x	Nitrogen oxides
SI	Spark Ignited
SOI	Start of Injection
TDC	Top Dead Centre
UHC	Unburned hydrocarbons
VEMOD	Virtual Engine Model
VGT	Variable Geometry Turbine
VVA	Variable Valve Actuation
VVT	Variable Valve Timing
WLTC	Worldwide Harmonized Light-Duty Vehicles Test Cycle

References

1. Arnau, F.J.; Martín, J.; Pla, B.; Auñón, Á. Diesel engine optimization and exhaust thermal management by means of variable valve train strategies. *Int. J. Engine Res.* **2020**. [CrossRef]
2. Luján, J.M.; Serrano, J.R.; Piqueras, P.; García-Afonso, Ó. Experimental assessment of a pre-turbo aftertreatment configuration in a single stage turbocharged diesel engine. Part 2: Transient operation. *Energy* **2015**, *80*, 614–627. [CrossRef]
3. Lancefield, T.; Methley, I.; Räse, U.; Kuhn, T. The Application of Variable Event Valve Timing to a Modern Diesel Engine. In Proceedings of the SAE 2000 World Congress, Detroit, MI, USA, 6–9 March 2000. [CrossRef]
4. Gonzalez, D.M.; Di Nunno, D. Internal Exhaust Gas Recirculation for Efficiency and Emissions in a 4-Cylinder Diesel Engine. In Proceedings of the SAE 2016 International Powertrains, Fuels and Lubricants Meeting, Baltimore, MD, USA, 24–26 October 2016. [CrossRef]
5. Serrano, J.R.; Piqueras, P.; Navarro, R.; Gómez, J.; Michel, M.; Thomas, B. Modelling Analysis of Aftertreatment Inlet Temperature Dependence on Exhaust Valve and Ports Design Parameters. In Proceedings of the SAE 2016 World Congress and Exhibition, Detroit, MI, USA, 12–14 April 2016. [CrossRef]
6. Siewert, R. How Individual Valve Timing Events Affect Exhaust Emissions. *SAE Trans.* **1971**. [CrossRef]
7. Tomoda, T.; Ogawa, T.; Ohki, H.; Kogo, T.; Nakatani, K.; Hashimoto, E. Improvement of Diesel Engine Performance by Variable Valve Train System. *Int. J. Engine Res.* **2010**, *11*, 331–344. [CrossRef]
8. Benajes, J.; Reyes, E.; Luján, J.M. Modelling Study of the Scavenging Process in a Turbocharged Diesel Engine with Modified Valve Operation. *Proc. Inst. Mech. Eng. Part C J. Mech. Eng. Sci.* **1996**, *210*, 383–393. [CrossRef]
9. Deppenkemper, K.; Özyalcin, C.; Ehrly, M.; Schoenen, M.; Bergmann, D.; Pischinger, S. 1D Engine Simulation Approach for Optimizing Engine and Exhaust Aftertreatment Thermal Management for Passenger Car Diesel Engines by Means of Variable Valve Train (VVT) Applications. In Proceedings of the WCX World Congress Experience, Detroit, MI, USA, 10–12 April 2018. [CrossRef]
10. Zammit, J.; McGhee, M.; Shayler, P.; Law, T.; Pegg, I. The effects of early inlet valve closing and cylinder disablement on fuel economy and emissions of a direct injection diesel engine. *Energy* **2015**, *79*, 100–110. [CrossRef]
11. Pan, X.; Zhao, Y.; Lou, D.; Fang, L. Study of the Miller Cycle on a Turbocharged DI Gasoline Engine Regarding Fuel Economy Improvement at Part Load. *Energies* **2020**, *13*, 1500. [CrossRef]
12. Piano, A. Analysis of Advanced Air and Fuel Management Systems for Future Automotive Diesel Engine Generation. Ph.D. Thesis, Politecnico di Torino, Torino, Italy, 2018.
13. Guan, W.; Pedrozo, V.B.; Zhao, H.; Ban, Z.; Lin, T. Variable valve actuation–based combustion control strategies for efficiency improvement and emissions control in a heavy-duty diesel engine. *Int. J. Engine Res.* **2019**. [CrossRef]
14. Guan, W.; Zhao, H.; Ban, Z.; Lin, T. Exploring alternative combustion control strategies for low-load exhaust gas temperature management of a heavy-duty diesel engine. *Int. J. Engine Res.* **2019**, *20*, 381–392. [CrossRef]
15. Maniatis, P.; Wagner, U.; Koch, T. A model-based and experimental approach for the determination of suitable variable valve timings for cold start in partial load operation of a passenger car single-cylinder diesel engine. *Int. J. Engine Res.* **2019**, *20*, 141–154. [CrossRef]
16. Kim, J.; Choongsik, B. An investigation on the effects of late intake valve closing and exhaust gas recirculation in a single-cylinder research diesel engine in the low-load condition. *Proc. Inst. Mech. Eng. Part D J. Automob. Eng.* **2016**, *230*, 771–787. [CrossRef]
17. Zhou, X.; Liu, E.; Sun, D.; Su, W. Study on transient emission spikes reduction of a heavy-duty diesel engine equipped with a variable intake valve closing timing mechanism and a two-stage turbocharger. *Int. J. Engine Res.* **2019**, *20*, 277–291. [CrossRef]
18. Gosala, D.B.; Ramesh, A.K.; Allen, C.M.; Joshi, M.C.; Taylor, A.H.; Voorhis, M.V.; Shaver, G.M.; Farrell, L.; Koeberlein, E.; James McCarthy, J.; et al. Diesel engine aftertreatment warm-up through early exhaust valve opening and internal exhaust gas recirculation during idle operation. *Int. J. Engine Res.* **2018**, *19*, 758–773. [CrossRef]

19. Parvate-Patil, G.; Hong, H.; Gordon, B. Analysis of Variable Valve Timing Events and Their Effects on Single Cylinder Diesel Engine. In Proceedings of the 2004 Powertrain and Fluid Systems Conference and Exhibition, Tampa, FL, USA, 25–28 October 2004. [CrossRef]
20. Piano, A.; Millo, F. Numerical Analysis on the Potential of Different Variable Valve Actuation Strategies on a Light Duty Diesel Engine for Improving Exhaust System Warm Up. In Proceedings of the 13th International Conference on Engines and Vehicles, Capri, Italy, 10–14 September 2017. [CrossRef]
21. Payri, F.; Arnau, F.; Piqueras, P.; Ruiz, M. Lumped Approach for Flow-Through and Wall-Flow Monolithic Reactors Modelling for Real-Time Automotive Applications. In Proceedings of the WCX World Congress Experience, Detroit, MI, USA, 10–12 April 2018. [CrossRef]
22. Martín, J.; Arnau, F.; Piqueras, P.; Auñón, A. Development of an Integrated Virtual Engine Model to Simulate New Standard Testing Cycles. In Proceedings of the WCX World Congress Experience, Detroit, MI, USA, 10–12 April 2018. [CrossRef]
23. Serrano, J.R.; Arnau, F.; García-Cuevas, L.; Dombrovsky, A.; Tartoussi, H. Development and validation of a radial turbine efficiency and mass flow model at design and off-design conditions. *Energy Convers. Manag.* **2016**, *128*, 281–293. [CrossRef]
24. Galindo, J.; Tiseira, A.; Navarro, R.; Tarí, D.; Tartoussi, H.; Guilain, S. Compressor Efficiency Extrapolation for 0D-1D Engine Simulations. In Proceedings of the SAE 2016 World Congress and Exhibition, Detroit, MI, USA, 12–14 April 2016. [CrossRef]
25. Serrano, J.R.; Olmeda, P.; Arnau, F.; Samala, V. A holistic methodology to correct heat transfer and bearing friction losses from hot turbocharger maps in order to obtain adiabatic efficiency of the turbomachinery. *Int. J. Engine Res.* **2020**, *21*, 1314–1335. [CrossRef]
26. Serrano, J.R.; Olmeda, P.; Arnau, F.J.; Dombrovsky, A.; Smith, L. Analysis and Methodology to Characterize Heat Transfer Phenomena in Automotive Turbochargers. *J. Eng. Gas Turbines Power* **2014**, *137*. [CrossRef]
27. Serrano, J.R.; Olmeda, P.; Arnau, F.J.; Dombrovsky, A.; Smith, L. Turbocharger heat transfer and mechanical losses influence in predicting engines performance by using one-dimensional simulation codes. *Energy* **2015**, *86*, 204–218. [CrossRef]
28. Arrègle, J.; López, J.J.; Martín, J.; Mocholí, E.M. Development of a Mixing and Combustion Zero-Dimensional Model for Diesel Engines. In Proceedings of the SAE 2006 World Congress and Exhibition, Detroit, MI, USA, 3–6 April 2006. [CrossRef]
29. Payri, F.; Arrègle, J.; López, J.J.; Mocholí, E. Diesel NOx Modeling with a Reduction Mechanism for the Initial NOx Coming from EGR or Re-entrained Burned Gases. In Proceedings of the SAE World Congress and Exhibition, Detroit, MI, USA, 14–17 April 2008. [CrossRef]
30. Broatch, A.; Olmeda, P.; Martín, J.; Salvador-Iborra, J. Development and Validation of a Submodel for Thermal Exchanges in the Hydraulic Circuits of a Global Engine Model. In Proceedings of the WCX World Congress Experience, Detroit, MI, USA, 10–12 April 2018. [CrossRef]
31. Guardiola, C.; Pla, B.; Bares, P.; Mora, J. An on-board method to estimate the light-off temperature of diesel oxidation catalysts. *Int. J. Engine Res.* **2018**. [CrossRef]
32. Russell, A.; Epling, W. Diesel Oxidation Catalysts. *Catal. Rev.* **2011**, *53*, 337–423. [CrossRef]
33. Guardiola, C.; Pla, B.; Piqueras, P.; Mora, J.; Lefebvre, D. Model-based passive and active diagnostics strategies for diesel oxidation catalysts. *Appl. Therm. Eng.* **2017**, *110*, 962–971. [CrossRef]
34. Abdelghaffar, W.A.; Osman, M.M.; Saeed, M.N.; Abdelfatteh, A.I. Effects of Coolant Temperature on the Performance and Emissions of a Diesel Engine. In Proceedings of the ASME 2002 Internal Combustion Engine Division Spring Technical Conference, Montreal, QC, Canada, 29 September–2 October 2002; Number ICES2002-464; pp. 187–197. [CrossRef]
35. Torregrosa, A.; Olmeda, P.; Martín, J.; Degraeuwe, B. Experiments on the influence of inlet charge and coolant temperature on performance and emissions of a DI Diesel engine. *Exp. Therm. Fluid Sci.* **2006**, *30*, 633–641. [CrossRef]